# HORIZONTAL CELLULAR STREAMING IN A STANDING SURFACE GRAVITY WAVE

Matsunaga, Nobuhiro
Department of Civil Engineering Hydraulics and Soil Mechanics, Kyushu University : Research Associate

Honji, Hiroyuki
Research Institute for Applied Mechanics, Kyushu University : Professor

https://doi.org/10.5109/6781008

出版情報：Reports of Research Institute for Applied Mechanics. 31 (98), pp.65-74, 1984-02. 九州大学応用力学研究所
バージョン：
権利関係：

Reports of Research Institute for Applied Mechanics
Vol. XXXI, No. 98, 1984

# HORIZONTAL CELLULAR STREAMING IN A STANDING SURFACE GRAVITY WAVE*

By Nobuhiro MATSUNAGA† and Hiroyuki HONJI‡

Along both side-walls of a wave tank, a region of horizontal, cellular, steady streaming is formed on and near the free surface of a fluid making a standing wave motion in the tank. Streamline patterns of this wave-induced streaming are computed by using a model, in which the fluid viscosity is considered only in the horizontal fluid motion. The computed streamline patterns agree qualitatively with observation.

***Key words*** : Standing wave, Induced streaming, Flow visualization

## 1. Introduction

Nonlinear effects combined with the action of viscosity in the standing waves in fluids set up steady streamings of the fluids. Of these, a well-known example is the acoustic streaming in Kundt's-tubes first studied by Rayleigh[1),2)]. Nonlinear wave-effects including the acoustic streaming are discussed in the context of waves in fluids in Tolstoy[3)] and Lighthill[4)].

Standing surface-gravity waves of water may also give rise to similar streamings. The purpose of this paper is to present the results of visual observations of a horizontal streaming induced on and near the free surface of water or glycerine-water solution making a standing gravity-wave motion in wave tanks with vertical side-walls, and of a model analysis of its streamline pattern.

## 2. Method of observations

Two wave tanks made of transparent plastic plates were used; one was 200 cm long, 15 cm wide, and 20 cm deep, and the other 300 cm long, 50 cm wide, and 20 cm deep. The experimental set-up with the shorter tank is illustrated in

* Presented March 19, 1982 at the Research Institute for Applied Mechanics, Kyushu University.

† Research Associate, Department of Civil Engineering Hydraulics and Soil Mechanics, Kyushu University.

‡ Professor, Research Institute for Applied Mechanics, Kyushu University.

figure 1. Standing waves were set up in the tanks by using a flap-type wave generator driven by a variable-speed motor, which was attached to one end of the tank. The frequency of flap oscillation ($f$) ranged from 1.3 to 2.3 Hz.

Water and glycerine-water solutions were used as a working fluid. The basic appearances of streaming patterns were the same for both fluids. When water was used, however, ripple waves were liable to disturb the formation of symmetric streaming patterns. Regular streaming patterns were formed easily in glycerin-water solutions because of the lesser background disturbances and the higher viscosity of the solutions. The kinematic viscosity ( $\nu$ ) of the solutions ranged from 0.26 to 0.40 cm$^2$/s. Streaming patterns visualised with tracer particles were photographed using a 35 mm camera placed above the tanks.

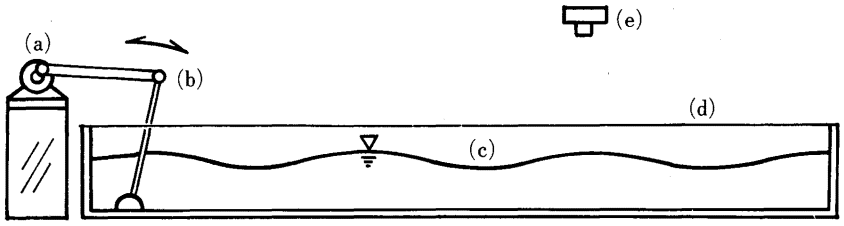


Figure 1. Experimental set-up.
(a) Motor, (b) wave-generating flap, (c) standing wave
(d) wave tank, (e) camera.

## 3. Results of observations

It has been observed that a steady streaming consisting of aligned vortices forms along the side-walls of a wave tank, when a standing wave motion has set up in the tank. Figure 2 shows a streaming induced on the surface of a glycerine-water solution; $L$, $2a$, and $h$, denote the wavelength, the wave hight, and the depth of fiuid, respectively. The streaming was visualised with aluminium particles scattered on the fluid surface. The cellular vortices forming the streaming aligned along a straight side-wall of the broad (50 cm wide) tank. The arrows indicate the positions of anti-node of the wave, where the fluid surface moves up and down and the streaming velocity is directed outwards from the tank-wall. The streaming was narrower and stronger at the wave anti-nodes. The streaming turned inwards to the tank-wall at the wave nodes where the fluid particles made a horizontal oscillatory motion. The cell size in the off-the-wall direction is about $L/2$. The streaming looked most conspicuous on the fluid surface and as attenuated downwards.

This picture was photographed after one minute from the start of the wave

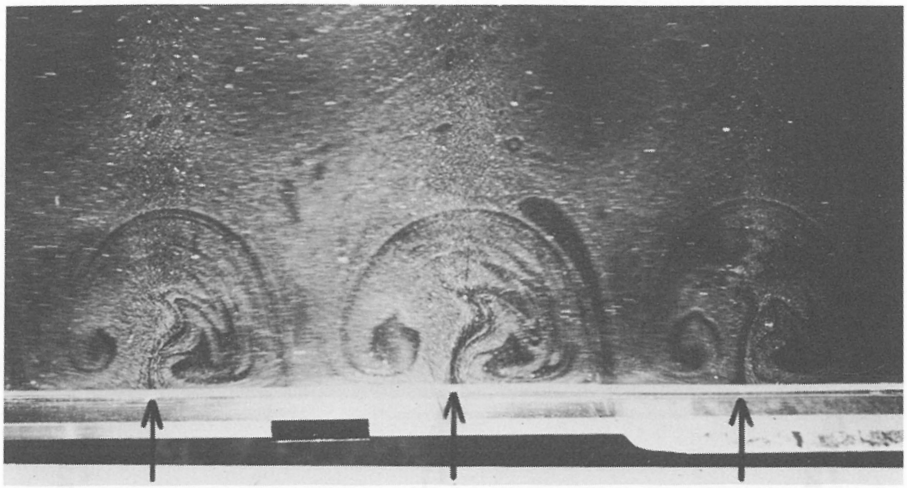

Figure 2. Plan view of induced streaming along a side-wall of broad wave-tank.
$f = 1.39$ Hz, $\nu = 0.41$ cm$^2$/s, $L = 52.0$ cm,
$2a = 2.4$ cm, $h = 16$ cm.

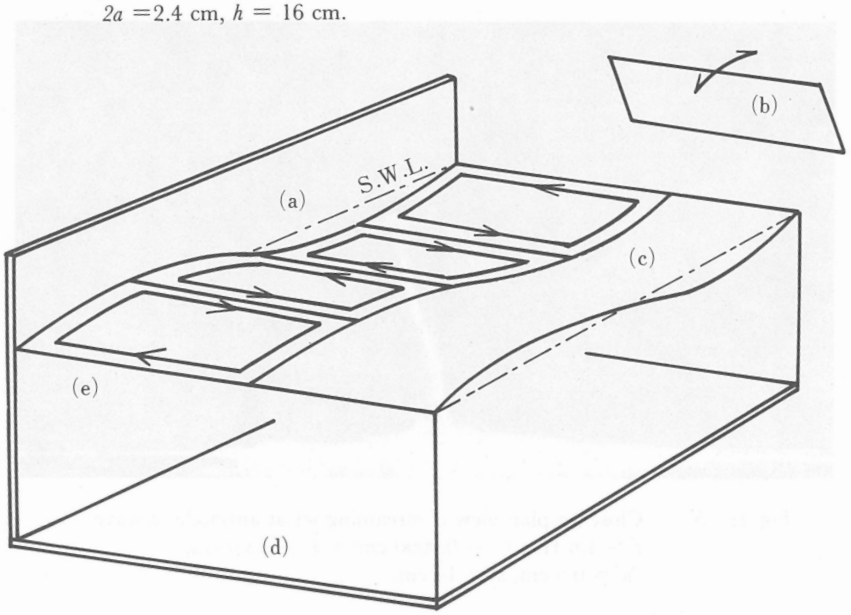


Figure 3. Schematic illustration of observed streaming region along a side-wall of wave tank.
(a) Side wall, (b) flap, (c) wave surface,
(d) bottom of tank, (e) streaming region.

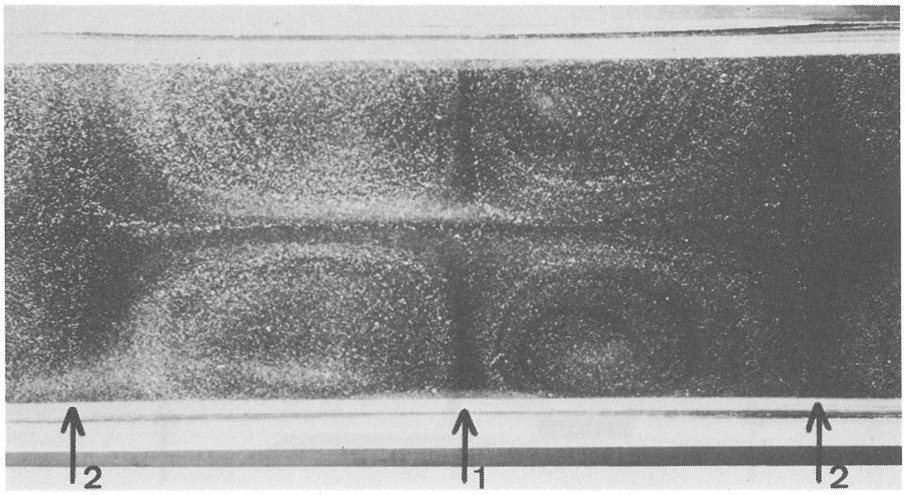


Figure 4. Plan view of induced streaming in narrow tank.
$f = 1.39$ Hz, $\nu = 0.26\text{cm}^2/\text{s}$, $L = 54.5$ cm,
$2a = 1.9$ cm, $h = 14$ cm.

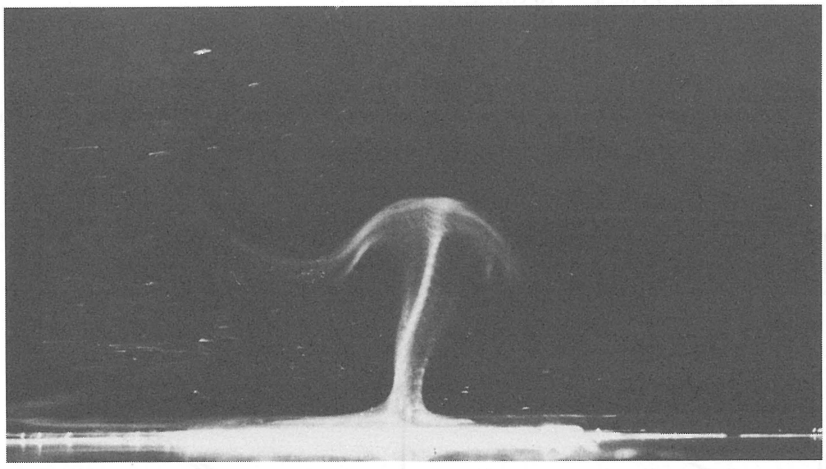

Figure 5. Close-up plan view of streaming jet at antinode of wave.
$f = 1.6$ Hz, $\nu = 0.0090\ \text{cm}^2/\text{s}$, $L = 53.0$ cm,
$2a = 0.5$ cm, $h = 14$ cm.

motion. After longer times, e.g. five minutes or more, the streaming was fairly distorted due to the diffusion of turbulence generated by the oscillating flap. However, the flow direction and the position of detachment of the outward streaming remained unchanged.

The observed streaming pattern is illustrated schematically in figure 3, where the flow directions are indicated by arrows. The fluid particles move away from the wall at every anti-node and turn inwards to the wall at every node of the wave. The streaming cells space at quarter-wavelength ($L/4$) intervals.

Figure 4 shows a steady streaming on the surface of a glycerine-water solution in a narrow (15 cm) tank. The streaming was visualised with small air bubbles trapped on the fluid surface. In the off-the-wall direction, the streaming cells formed along both side-walls of the tank were squeezed into the narrow space of the tank. The symmetric streaming was not distorted in this case, except in the region near the flap. Arrow 1 indicates the wave antinode where the fluid particles move away from the wall, and arrow 2 the wave node where they turn into the wall.

Similarly as in the case of the broad tank four streaming cells form within one wavelength, but the cell size in the off-the-wall direction is narrowed dowm to half the width of the tank. Figure 5 shows a streaming in which the fluid particles are moving away from the wall of the same tank at an anti-node of the wave. The working fluid was water, and only one side of the streaming at about 1 cm below the free water surface was visualised with a dye tracer. The visualised streaming forms a jet directed outwards from the wall.

## 4. Model analysis and discussion

A model analysis of streamline patterns of the induced streaming in a broad and infinitely deep tank is carried out based on a perturbation method applied to the viscous flow equation. As illustrated in figure 6, take axes $(x', y', z')$ horizontal along, normal to, and downwards along the inside surface of a tank wall, respectively, with the origin $O$ at the still water level. The displacement ($\eta$) of the surface of a standing wave extending in the $x'$-direction is expressed as

$$\eta = a \cos kx' \cos \omega t' \qquad (1)$$

where $k = 2\pi/L$, $\omega$ is the wave angular frequency, and $t'$ is the time. The velocity potential ($\Phi'$) of the wave is expressed as

$$\Phi' = -\frac{a\omega}{k} e^{-kz'} \cos kx' \sin \omega t' \qquad (2)$$

The effects of viscosity on the fluid motion are predominant near the walls. We assume that only the potential flow components in the $(x', y')$ plane are modified by the viscous effects, and denote the $(x', y', z')$ components of the flow velocity as

$$u' = \frac{\partial \Phi'}{\partial x'} + \frac{\partial \Psi'}{\partial y'},$$

$$v' = -\frac{\partial \Phi'}{\partial x'}, \qquad (3)$$

$$w' = \frac{\partial \Phi'}{\partial z'},$$

where $\Psi'$ is the stream function associated with the viscous effects at constant $z'$. Under the above assumption, this model allows the slip velocity $w'$ on the wall. These equations are substituted into the two-dimensional viscous flow equation with the pressure term eliminated

$$\frac{\partial}{\partial t'}\left(\frac{\partial u'}{\partial y'} - \frac{\partial v'}{\partial x'}\right) + u'\frac{\partial}{\partial x'}\left(\frac{\partial u'}{\partial y'} - \frac{\partial v'}{\partial x'}\right) +$$

$$v'\frac{\partial}{\partial y'}\left(\frac{\partial u'}{\partial y'} - \frac{\partial v'}{\partial x'}\right) = \nu\left(\frac{\partial^2}{\partial x'^2} + \frac{\partial^2}{\partial y'^2}\right)\left(\frac{\partial u'}{\partial y'} - \frac{\partial v'}{\partial x'}\right) \qquad (4)$$

to obtain

$$\frac{\partial}{\partial t'}(\nabla'^2\Psi') + \left(\frac{\partial \Phi'}{\partial x'} + \frac{\partial \Psi'}{\partial y'}\right)\frac{\partial}{\partial x'}(\nabla'^2\Psi') -$$

$$\frac{\partial \Psi'}{\partial x'}\frac{\partial}{\partial y'}(\nabla'^2\Psi') = \nu\ \nabla'^4\Psi', \qquad (5)$$

where $\nabla'^2 = \dfrac{\partial^2}{\partial x'^2} + \dfrac{\partial^2}{y'^2}$.

The boundary conditions are

$$y' = 0\ ;\ \frac{\partial \Psi'}{\partial y'} = -\frac{\partial \Phi'}{\partial x'},\ -\frac{\partial \Psi'}{\partial x'} = 0,$$

$$y' \to \infty\ ;\ \frac{\partial \Psi'}{\partial y'} = -\frac{\partial \Psi'}{\partial x'} = 0. \qquad (6)$$

We introduce $\delta$ and the non-dimensional quantities $x, y, z, t, \Psi, \Phi, \alpha$, and $\epsilon$ as follows

$$x' = k^{-1}x,\ y' = \delta y,\ z' = k^{-1}z,\ t' = \omega^{-1}t,\ \Psi' = \alpha\omega\delta\Psi,$$

$$\Phi' = \alpha\omega\delta\Phi,\ \ \delta = (2\nu/\omega)^{1/2},\ \ \alpha = \delta k,\ \ \epsilon = \alpha k. \qquad (7)$$

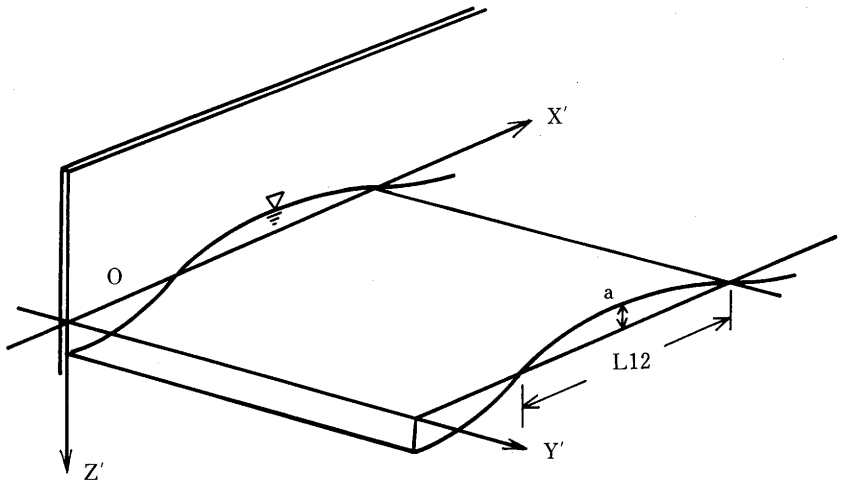


Figure 6. Coordinate system.

In terms of these non-dimensional quantities, the basic equation and the boundary conditions can be written as

$$\frac{\partial}{\partial t}(\nabla^2\Psi) + \varepsilon \left[\{e^{-z}\sin x \sin t + \frac{\partial \Psi}{\partial y}\} \frac{\partial}{\partial x}(\nabla^2\Psi) - \frac{\partial \Psi}{\partial x}\frac{\partial}{\partial y}(\nabla^2\Psi)\right] = \frac{1}{2}\nabla^4\Psi , \tag{8}$$

where $\nabla^2 = \alpha^2 \frac{\partial^2}{\partial x^2} + \frac{\partial^2}{y^2}$, and

$$y = 0 ; \frac{\partial \Psi}{\partial y} = -e^{-z}\sin x \sin t , \frac{\partial \Psi}{\partial x} = 0 ,$$
$$y \to \infty ; \frac{\partial \Psi}{\partial y} = \frac{\partial \Psi}{\partial x} = 0 . \tag{9}$$

Assuming $\varepsilon \ll 1$, we expand $\Psi$ as

$$\Psi = \Psi_0 + \varepsilon \Psi_1 + \cdots\cdots \tag{10}$$

and calculate the steady part $\Psi_{1s}$ in $\Psi_1$ .
There result for $\Psi_0$ and $\Psi_{1s}$,

$$\Psi_0 = \mathrm{Re}\ [\{A_0 e^{-\alpha y} + B_0 e^{-\sigma y}\}\ \sin x\, e^{it}]\ , \qquad (11)$$

with $A_0 = \dfrac{-i\, e^{-z}}{\alpha - \sigma}$, $B_0 = \dfrac{i e^{-z}}{\alpha - \sigma}$,

$$\sigma = (\alpha^2 + 2i)^{1/2},$$

and

$$\Psi_{1s} = \mathrm{Re}\ [f_{1s}(y) \sin 2x]\ , \qquad (12)$$

with

$$f_{1s}(y) = A_1 e^{-\sigma^* y} + B_1 e^{-(\alpha+\sigma^*)y} + C_1 e^{-(\alpha+\sigma^*)y} + (D_1 y + E_1) e^{-2\alpha y},$$

$$A_1 = -\frac{B_0^* e^{-z}}{(\sigma^{*2} - 4\alpha^2)^2}\ ,$$

$$B_1 = \frac{i A_0 B_0^* (\alpha - \sigma^*)}{\{(\alpha + \sigma^*)^2 - 4\alpha^2\}^2}\ ,$$

$$C_1 = \frac{i B_0 B_0^* (\sigma - \sigma^*)}{\{(\sigma + \sigma^*)^2 - 4\alpha^2\}^2}\ ,$$

$$D_1 = (\sigma^* - 2\alpha) A_1 + (\sigma^* - \alpha) B_1 + (\sigma + \sigma^* - 2\alpha) C_1\ ,$$

$$E_1 = -(A_1 + B_1 + C_1),$$

where Re denotes 'real part of', $i$ the complex operator, and the asterisk the complex conjugate. The distribution of shear stresses ($\tau$) on the surface of the tank wall is also computed based on the equation

$$\tau = \frac{\partial^2 \Psi_{1s}}{\partial y^2}\Big|_{y=0}\ . \qquad (13)$$

An example of computed patterns is presented in figure 7. In the figure, $x = 0$, $\pi$, and $2\pi$ correspond to the wave anti-nodes, and $x = \pi/2$ and $3\pi/2$ to the nodes. Four streaming cells are formed within one wavelength between $x = 0$ and $2\pi$. The cell size in the direction normal to the wall is about half the wavelength. Also presented is the distribution of $\tau$, where $\tau > 0$ and $\tau < 0$ indicate the positive and negative flow directions of the streaming near the wall, respectively. This figure shows that the streaming is outwards from the wall at wave anti-nodes and inwards to the wall at nodes. The cell size and the streaming direction agree with the results of observation described in the preceding section.

A remark should be made here on a possible connection of this type of streaming with the nearshore cell circulation. The mechanism of streaming generation in a standing wave seems similar to that in a standing edge wave. Thus, the induced streaming so far discussed may be regarded as a rip current, which plays an essential role in the analysis of coastal flow systems.

We would like to thank Prof. T. Tsubaki and Dr A. Kaneko for stimulating discussions. We are indebted to Mr Y. Shiraishi for technical help. The work was supported by a Ministry of Education grant, which is gratefully acknowledged. The computation was carried out using the RIAM MELCOM-COSMO 900 computer.

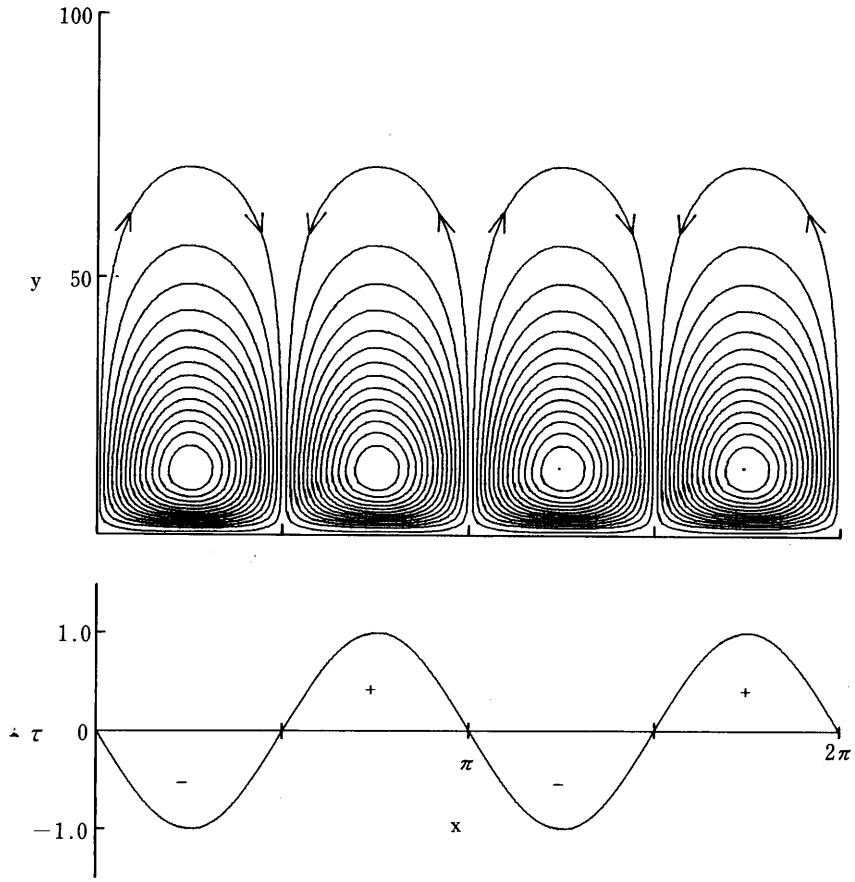


Figure 7. Computed streamlines and wall-shear distribution for induced streaming : $\tau$ is normalized by its maxium value.

## References

1) Rayleigh, J. W. S.: On the Circulation of Air Observed in Kundt's Tubes, and on Some Allied Acoustical Ploblems, Phil. Trans. Roy. Soc. London **175** (1883) 1–21.
2) Rayleigh, J. W. S.: *The Theory of Sound,* Vol. 2, 1945, Dover, N. Y.
3) Tolstoy, I.: *Wave Propagation,* 1973, McGraw-Hill.
4) Lighthill, J.: *Waves in Fluids,* 1978, Cambridge Univ. Press.

(Received November 25, 1983)